

www.acsami.org Research Article

Polymer Precursor Derived Li_xPON Electrolytes: Toward Li-S Batteries

Eleni Temeche, Xinyu Zhang, and Richard M. Laine*



Cite This: ACS Appl. Mater. Interfaces 2020, 12, 20548–20562



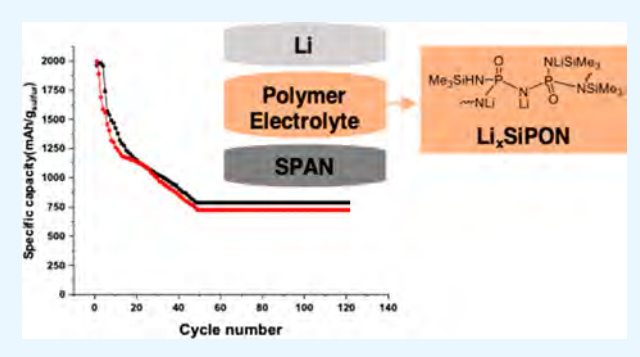
ACCESS

Metrics & More

Article Recommendations

Supporting Information

ABSTRACT: Efforts to develop polymer precursor electrolytes that offer properties anticipated to be similar or superior to (lithium phosphorus oxynitride, LiPON) glasses are reported. Such precursors offer the potential to be used to process LiPON-like thin glass/ceramic coatings for use in all solid state batteries, ASBs. Here, LiPON glasses provide a design basis for the synthesis of sets of oligomers/polymers by lithiation of $OP(NH_2)_{3-x}(NH)_x$ [from $OP(NH)_3$], $OP(NH_2)_{3-x}(NHSiMe_3)_x$ and $[P=N]_3(NHSiMe_3)_{6-x}(NH)_x$. The resulting systems have degrees of polymerization of 5-20. Treatment with selected amounts of LiNH₂ provides varying degrees of lithiation and Li⁺ conducting properties commensurate with Li⁺ content. Polymer electrolytes impregnated in/on Celgard exhibit Li⁺ conductivities up



to $\sim 1 \times 10^{-5} \mathrm{S} \ \mathrm{cm}^{-1}$ at room temperature and are thermally stable to $\sim 150 \ ^{\circ}\mathrm{C}$. A Li–S battery assembled using a Li₆SiPON composition polymer electrolyte exhibits an initial reversible capacity of 1500 mAh g_{sulfur}^{-1} and excellent cycle performance at 0.25 and 0.5 C rate over 120 cycles at room temperature.

KEYWORDS: Li,PON, Li,SiPON, Li,SiPHN, polymer precursors, electrolytes, Celgard, Li-S batteries

1. INTRODUCTION

Traditional Li⁺ batteries employ molecular electrolytes dissolved in organic solvents imposing battery design and size restrictions that have inherent safety risks and constrain service temperatures.^{1,2} In contrast, solid-state electrolytes offer the potential to reduce overall battery footprints thereby increasing energy densities coincident with improved safety.^{3–5} However, most solid electrolytes suffer from low ionic conductivities or limited stability windows. Lithium phosphorus oxynitride glass (LiPON) is a commonly used solid-state electrolyte. Since its discovery in the early 1990s by Bates et al.,^{6,7} the material has received increasing attention due to its broad electrochemical stability window (0–5 V vs Li⁺/Li),^{8–10} reasonable conductivity (10^{–6} S cm^{–1}),^{8–11} and negligible electronic conductivity (10^{–7} μS cm^{–1}).^{1,10}

LiPON solid electrolytes enable ASB thin film batteries. LiPON thin films are typically processed by radio frequency magnetron sputtering (RFMS) deposition of lithium silicates and lithium phosphate in Ar or N₂ atmospheres. LiPON other synthesis methods include pulse laser deposition (PLD), lectron-beam (EB) evaporation, lectron-beam assisted deposition (IBAD), lectron beam sputtering (IBS), and plasma-enhanced metallo-organic chemical vapor deposition (MOCVD). LiPON materials produced by vacuum deposition.

The main limitation to gas phase deposition methods centers on their low deposition rates limiting their utility for fabricating large surface area substrates or multiple targets simultaneously. For example, RFMS deposition rates are often <3.0 nm min⁻¹, ¹², ¹⁶, ¹⁹ PLD films deposition rates range from 13.3 to 50 nm min⁻¹, ^{13,16} while those processed using IBAD can approach 70 nm min^{-1,15,16} Additionally, controlling the extent and uniformity of Li₃PO₄ nitridation can be challenging. Sputtering is also limited to depositing high quality films on 3D geometries.²⁰ To overcome these obstacles, researchers have been developing alternative deposition techniques, i.e., atomic layer deposition (ALD) for fabrication of uniform, thin, and conformal LiPON films. 21 Unfortunately, these methods all require a specialized apparatus to control deposition atmospheres, rates, film properties, and coating uniformity. As such, they represent an expensive step in fabricating ASBs which makes it challenging for commodity applications.

In contrast, polymer precursors that melt or are soluble offer a facile, low cost alternative as they permit application in liquid format; easy to control and scale. Polymer precursor methods

Received: February 24, 2020 Accepted: April 13, 2020 Published: April 13, 2020





Table 1. Examples of LiPON Thin Coating Processes and Properties

| composition | N/P ratio | synthesis method | thickness | conductivity ^a (S/cm) | ref. |
|--|-----------|---|----------------------|----------------------------------|------|
| Li _{3.3} PO _{3.8} N _{0.24} to Li _{3.6} PO _{3.3} N _{0.69} | 0.24-0.69 | RFMS of a Li ₃ PO ₄ target in N ₂ | 1 μm | $2 (\pm 1) \times 10^{-6}$ | 8 |
| Li _{3.3} PO _{2.1} N _{1.4} | 1.4 | RFMS of a Li ₃ PO ₄ target in N ₂ | $1~\mu\mathrm{m}$ | 1.8×10^{-6} | 12 |
| LiPON | N/A | PLD | $1-3 \mu m$ | 1.6×10^{-6} | 13 |
| LiPON | N/A | EB evaporation of Li ₃ PO ₄ in ionized N ₂ | N/A | 6.0×10^{-7} | 14 |
| LiPON (Y290, Y301) | N/A | IBAD of thermally evaporated Li ₃ PO ₄ | $1.05~\mu\mathrm{m}$ | Y290: 1.3×10^{-6} | 15 |
| | | | | Y301: 9.0×10^{-7} | |
| LiPON | 0.39-1.49 | PA-DVD | $0.3-2 \ \mu m$ | $10^{-7} - 10^{-8}$ | 16 |
| Ultrathin LiPON | N/A | IBS | ≥12 nm | $1-2 \times 10^{-7}$ | 17 |
| $Li_{2.9}PO_{4.5}N_{0.42} \ to \ Li_{3.1}PO_{4.1}N_{0.42}$ | 0.42 | MOCVD | N/A | $2.75 - 2.95 \times 10^{-7}$ | 18 |
| ^a Conductivity at room temperature | e. | | | | |

of processing ceramics are the subject of multiple reviews. $^{22-26}$ However, to our knowledge, no one has sought to apply this approach to processing thin Li_xPON films for battery applications. This then represents the motivation for the work reported here: to develop and optimize scalable precursors to $\text{Li}_x\text{PON-like}$ materials that overcome the above-mentioned obstacles.

Additionally, studies have shown that doping Li_xPON with Si improves ionic conductivity. $^{6,27-29}$ Lee et al. 27,28 report that introducing Si lowers activation energies increasing conductivities up to 10^{-5} S cm $^{-1}$. Su et al. 29 prepared Li_xSiPON with different compositions by RFMS. The highest conductivity found at ambient was $\sim 1 \times 10^{-5}$ S cm $^{-1}$ with an activation energy ~ 0.41 eV at Si:P = 1:1. This provides the impetus to include Li_xSiPON precursors in our repertoire as presented below.

Furthermore, if we assume that oxygens with two lone electron pairs and higher electronegativity may bind Li⁺ more tightly than nitrogen with only one electron pair and a lower electronegativity, then it seems logical to explore using a polymer based solely on phosphorus and nitrogen leading to our studies on Li_{*}SiPHN precursors.

Thus, LiPON glasses provide a design basis for synthesizing sets of oligomers/polymers by lithiation of $OP(NH_2)_{3-x}(NH)_x$ [from $OP(NH)_3$], $OP(NH_2)_{3-x}(NHSiMe_3)_x$, and $[P=N]_3(NHSiMe_3)_{6-x}(NH)_x$. The resulting systems have degrees of polymerization of 5–20. Treatment with selected amounts of LiNH₂ provides varying degrees of lithiation and Li⁺ conductivities commensurate with Li⁺ content. The objective here was to characterize the electrochemical and physical properties of the polymers through electrochemical impedance (EIS), thermogravimetric analysis (TGA), X-ray diffraction (XRD), Fourier-transform infrared spectroscopy (FTIR), matrix-assisted laser desorption/ionization (MALDI), and X-ray photoelectron spectroscopy (XPS).

Coincidentally we explored using these Li_xPON emulating oligomers/polymers as Li^+ electrolytes and as stable interface between Li and a sulfur-based cathode (SPAN). The theoretical energy density of Li–S systems (~2600 Wh kg⁻¹)³¹ is 5× higher than traditional Li-ion systems. S²⁻³⁴ The combination of abundant, inexpensive, nontoxic, and environmentally attractive features makes Li/S a promising next-generation energy storage technology. The stability of the Li–S cell at high c-rates (0.5C) and over long cycle times (>120) appears to arise, at least in part due to the electrochemical stability of the Li_xSiPON emulating polymer electrolyte.

2. EXPERIMENTAL SECTION

The first step in developing precursors is to realize simple, low cost, minimal step syntheses easily modified to allow exploration and thereafter control of both precursor properties and processing conditions. The following briefly describes our exploration of selected synthetic approaches.

2.1. Preparation of Polymer Precursors. Phosphorus oxychloride (OPCl₃) and hexamethyldisilazane $[NH(SiMe_3)_2]$ were obtained from Alfa Aesar. Sodium amide $(NaNH_2)$ and lithium amide $(LiNH_2)$ were obtained from Acros Organics. Hexachlorophosphazene $(Cl_6N_3P_3)$ was purchased from abcr GmbH. All chemicals were used as-received. All reactions were conducted under N_2 .

The polymer precursors are synthesized in two steps. The first step is to substitute the -Cl in the phosphorus source (OPCl $_3$ or $\text{Cl}_6\text{N}_3\text{P}_3$) with $-\text{NH}_2$ (from NaNH $_2$) or $-\text{NHSiMe}_3$ [from NH(SiMe $_3$) $_2$] producing byproduct NaCl or Me $_3$ SiCl (Table S1 of the Supporting Information, S1). It is followed by lithiation from the lithium source LiNH $_2$. Table S2 lists LiNH $_2$ amounts and properties of assynthesized precursors. Distilled Tetrahydrofuran (THF) is used as the solvent. All syntheses are done under N $_2$ in Schlenk flasks. The detailed polymer precursor synthesis can be found elsewhere. 38

On the basis of precursor design criteria described previously, 22,39 three LiPON-like precursors were synthesized. The simplest approach uses oligomeric $OP(NH_2)_3$ which, following lithiation, has only those elements needed to produce LiPON. A second precursor incorporates Si for the reasons noted above. $^{6,27-29}$ The third precursor was synthesized from the chlorophosphazene $[Cl_2P=N]_3$ eliminating all oxygen but also incorporating Si.

2.1.1. Synthesis of PON and Li_x PON Precurors. The simplest synthetic approach is ammonolysis of OPCl₃ forming phosphoramide OP(NH₂)₃ as shown in Scheme 1.

Scheme 1. Ammonolysis of OPCl₃

However, depending on the solvent, by product $\mathrm{NH_4Cl}$ is difficult to remove/interferes with purification. An alternative uses $\mathrm{NaNH_2}$ as shown in Scheme 2.

 $NaNH_2$ rather than $LiNH_2$ is used because LiCl is more soluble in polar solvents than NaCl and may not precipitate as easily and thus, $NaNH_2$ is preferable.

Thereafter, there are two options for producing LiPON precursors. The first is to promote ol-igomerization/polymerization following

Scheme 2. Reaction of OPCl₃ with NaNH₂

$$\begin{array}{c} O \\ \parallel \\ CI \\ CI \end{array} + 3NaNH_{2} \\ \begin{array}{c} O \\ \parallel \\ H_{2}N \\ H_{2}N \end{array} + 3NaCI$$

Scheme 3. Linear Oligomerization/Polymerization of OP(NH₂)₃ forming PON Precursor

Scheme 4. Branched or Cyclomeric Products on Heating of OP(NH₂)₃

reactions shown as stepwise condensation reactions presented in Scheme 3.

As shown in Scheme 4, only linear oligomers are formed. However, it is highly likely that both branched and cyclomeric products arise coincidentally.

The volatile system might offer a novel method for chemical vapor deposition. At this juncture, it is possible to now add Li as shown in Scheme 5.

Scheme 5. Lithiation of PON

As an alternative, our preferred choice is to do this right after the first step. This may not be optimal, but it appears to be the easiest approach as shown in Scheme 6.

The Li content can be controlled by the degree of initial lithiation. One can also envision promoting a condensation reaction as suggested in a simple fashion above. The condensation process is likely more complex than shown. However, one can use these intermediates as precursors to make LiPON thin films, binders, or bonding agents by using traditional precursor processing techniques. ^{22,39} In some instances, the intermediates will be liquids and in others, they will be meltable or soluble solids. As demonstrated below it is possible to make Li₃PON and Li₆PON precursors simply by choosing the amount of LiNH₂ to add.

2.2. Polymer Precursors to Li_xSiPON. As noted above, a few reports describe silicon containing LiPON or LiSiPON.^{6,27–29} To our knowledge, LiSiPON precursors have not been synthesized via the route shown in Scheme 7, which takes advantage of the affinity of Si for Cl.

A modified route uses (Scheme 8) less than 2.5 (Me₃Si)₂NH.

One can envision promoting polymerization using less $(Me_3Si)_2NH$ (≥ 1.5), forming SiPON precursor. At this stage, one can lithiate as shown in Scheme 9, and then warm as suggested below, which is not likely the only reaction pathway as presented in Scheme 10

The resulting material compositions will depend on the amount of ${\rm LiNH_2}$ and method of processing. The conductivity will be determined by this as well.

2.2.1. SiPHN and Li_x SiPHN Systems. To investigate the use of a polymer solely based on phosphorus and nitrogen, one can envision

Scheme 7. Reaction of OPCl₃ with (Me₃Si)₂NH (Mole Ratio = 1:3)

$$\begin{array}{c|c} O & O & O \\ \hline P & O & O \\ \hline CI & +3(Me_3Si)_2NH & \hline \\ & & & \\ \hline & & \\ & &$$

Scheme 8. Reaction of OPCl₃ with (Me₃Si)₂NH (mole ratio = 1:2.5)

starting from the commercial cyclomer: $[Cl_2P=N]_3$, replacing Cl with NH via the Si–Cl exchange process, followed by lithiation with LiNH₂ as demonstrated in Scheme 11.

As detailed in the Experimental Section, we followed this approach in formulating systems as illustrated, targeting processable polymers by using nonstoichiometric amounts of $(Me_3Si)_2NH$.

In this work, "x" in Li_xPON, Li_xSiPHN, and Li_xSiPON stands for the Li content, which is based on the theoretical Li/P ratios of the corresponding precursor.

2.3. Cell Fabrication. Celgard separators were purchased from (MTI, Richmond, CA). Celgard separator (25 μ m × 12 mm diameter) substrates were dip-coated for 1 min in Li₃PON (0.05 g mL⁻¹), Li₆PON (0.05 g mL⁻¹), Li₂SiPHN (0.08 g mL⁻¹), Li₃SiPON (0.1 g mL⁻¹), and Li₆SiPON (0.1 g mL⁻¹) solutions. These experiments were conducted to measure coating impedances without heat treatments; similar to measuring the impedance of conventional liquid electrolyte-soaked separators. The total conductivity [$\sigma_t = T/(A \times R)$], where T is the thickness of the Celgard, A is the contact area between the Celgard and the stainless steel (SS) disk (diameter = 16 mm), and R is the total resistivity obtained from the straight line of the real axes from the Nyquist plot.⁴⁰

2.3.1. Electrochemical Characterization. The electrochemical compatibility of the polymer precursor solutions in THF (20 μ L) was investigated using EIS of the stainless steel (SS)/Celgard + polymer precursor/SS with a potential amplitude of 10 mV from 0.1 to 100 kHz. The electrochemical stability of the polymer precursor was investigated by linear sweep voltammograms, which was obtained on a Biologics instrument at a scanning rate of 1 mV s⁻¹, where the polymer precursor coated Celgard was sandwiched between lithium anode and SS.

Scheme 6. Lithiation of OP(NH₂)₃ Followed by Oligomerization/Polymerization, Forming LiPON Precursor

Scheme 9. Lithiation of SiPON

Scheme 10. Oligomerization/Polymerization Forming LiSiPON Precursor

Scheme 11. Synthesis of LiSiPHN Precursor

To further assess polymer electrochemical properties, symmetric cells were assembled to study the effects of current density on the stability and kinetics of the Li/polymer electrolyte interface. Before cell assembly, the metallic Li (~2 cm²) was scraped exposing a clean surface. Symmetric and half coin cells were constructed using the standard procedure and compressed at ~0.015 psi using digital pressure controlled electric crimper (MTI, Richmond, CA). The Celgard was dip-coated for 1 min in Li₃PON (0.05 g mL $^{-1}$), Li₆PON (0.05 g mL $^{-1}$), Li₂SiPHN (0.08 g mL $^{-1}$), Li₃SiPON (0.1 g mL $^{-1}$), and Li₆SiPON (0.1 g mL $^{-1}$) polymer precursor solutions and heated to 90 °C/12 h/vacuum prior to half and symmetric cell assembly. Furthermore, polymer precursors in THF solution (20 μ L) were also

used as an additional electrolyte to wet the surface of the electrodes. The Li/Celgard + polymer precursor/Li symmetric cells were cycled at room temperature at the desired current densities of ($\pm 0.1-7.5$ mA) with a rest period of 10 min between each current step. The Li metal, polymer electrolytes, Celgard, and SPAN were stored in an argon filled glovebox (MBRAUN) with an average $\rm H_2O$ and $\rm O_2$ content below 0.1 ppm.

The SPAN electrode was prepared by coating 70:15:15 wt % mixture of SPAN/C65/PVDF in NMP on carbon coated Al foil. The cathode was then vacuum-dried at 60 °C. After drying the electrode, 14 mm in diameter SPAN were punched out and transferred to coin cells. The SPAN/Li₆SiPON/Li half-cell was charged and discharged to the cutoff voltages of 1-3 V using 0.5 C rate. Specific capacities were calculated based on the mass of sulfur in the cathode (1C = 1672 mAh g^{-1}).

3. RESULTS AND DISCUSSION

In the following section, we briefly characterize the polymer precursors, a more detailed description is available elsewhere.³⁸ We first monitored compositional and structural changes caused by the degree of lithiation and by the addition of silicon. The extent of lithiation and nitrogen content and its effect on the structure are discussed.

Table 2. MWs, CYs, and Estimated Compositions of Polymer Precursors

| Poly mer precursor | M W ^[a] , kDa | No. monomer units ^[b] | CY ^[c] , | $T_d(5\%)^{[d]}, {^{\circ}C}$ | $T_m^{[e]}$, $^{\circ}C$ | Likely monomer structures ^[f] |
|-----------------------|-----------------------------|--|---------------------|-------------------------------|---------------------------|--|
| Li ₃ PON | 0.6-1.4 | 5-15 | 50-60 | 150-180 | 560-580 | |
| Li ₆ PON | 0.6-1.9 | 5-20 | 50-60 | 150-180 | 570-590 | THE STATE OF THE S |
| | | | | | | Me ₃ Si — X |
| Li ₂ SiPHN | 0.7-1.5 | 2-4 | 45-55 | 140-160 | ≈600 | Me ₃ Si — X N N X N SiMe ₃ |
| | | | | | | Me ₃ Si N XN SiMe ₃ |
| Li ₃ SiPON | 0.5-1.0 | 5-13 | 45-60 | 150-200 | ≈600 | |
| | | | | | | XHN Me ₃ SiXN |
| Li ₆ SiPON | 0.7-1.5 | 6-15 | 50-65 | 150-170 | ≈600 | $\begin{bmatrix} \times & \overset{X}{N} & \overset{Y}{N} \end{bmatrix}$ $\begin{bmatrix} \overset{X}{N} & \overset{Y}{N} \end{bmatrix}$ |
| | | | | | | |

 a MW = molecular weight. b Number monomer units calculated based on MALDI. c CY = ceramic yield in TGA (800 $^\circ$ C/N₂). d T_d (5%) = 5% mass loss temp. in TGA (N₂/10 $^\circ$ C/min). e T_m = endotherm with no associated mass loss in DTA (N₂/10 $^\circ$ C/min). f X = H or Li

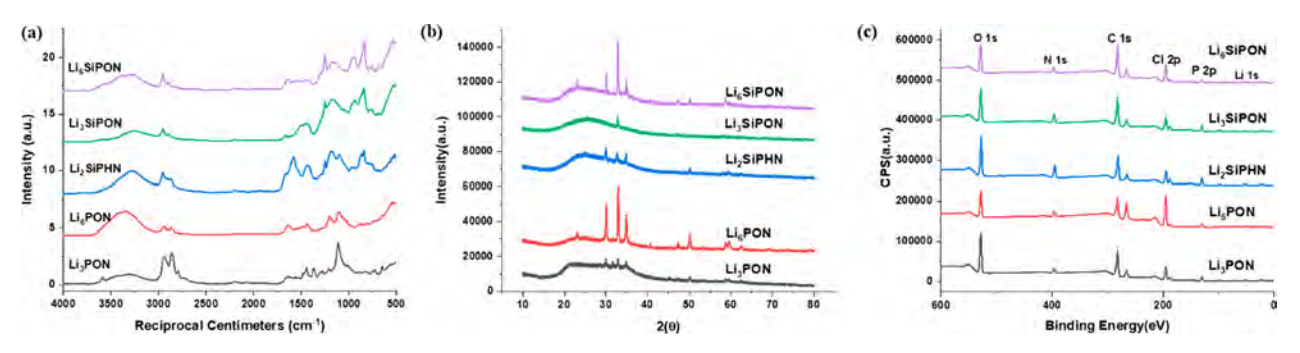


Figure 1. (a) FTIR spectra, (b). XRD. (C). and XPS of Li_xPON, Li_xSiPHN, and Li_xSiPON precursors.

3.1. Characterization of Polymer Precursors. GPC, MALDI-ToF, and TGA-DTA (800 °C N_2^{-1}) studies of polymer precursors are given in the SI (Figures S1–S5 and Tables S3–S5), detailed discussion are provided in a complementary manuscript.³⁸ Table 2 compares the MWs, ceramic yields (CYs), and likely structural components of the polymers based on GPC, MALDI, and TGA-DTA studies. All the polymers have similar CYs of 45–65 wt %. In general, CYs improve with increases in MWs.

Figure 1(a) shows the FTIR of representative as-synthesized precursors. Table S6 summarizes literature reported FTIRs of LiPON glasses. Typically, the precursors exhibit ν N–H (~3000 cm⁻¹, ~1500 cm⁻¹), ν P=O (1150–1300 cm⁻¹), ν P-O⁻ (1000–1150 cm⁻¹), ν P-N=P (800–900 cm⁻¹) and ν P-O-P (1150, 780–680 cm⁻¹) absorptions. ^{18,41–46} A small peak at ~2200 cm⁻¹ is also observed for all the precursors; suggested by Pichonat et al. ⁴⁵ and Stallworth et al., ⁴⁶ to arise from P-N < $_{P}^{p}$ or P-N=P bonds. Additionally, Si-containing precursors exhibit ν C-H at ~2950 cm⁻¹ from SiMe₃ groups. Precursor FTIR often present ν O-H at ~3400 cm⁻¹, likely from unreacted LiNH₂ that reacts with trace moisture forming LiOH. FTIR spectra recorded with stringent control of atmosphere during sample preparation show reduced ν O-H intensities.

The Li₃PON, Li₆PON, Li₂SiPHN, Li₃SiPON, and Li₆SiPON precursors were heated to 60 °C/Vacuum to remove solvent. Dried powders (1 g) were pelletized (3 mm diameter die). Pellets were heated between alumina plates to 100 °C/2 h/1 °C min⁻¹/120 mL min⁻¹ N₂. XRDs of Li₃PON, Li₂SiPHN, and Li₃SiPON show low intensity peaks ~30°, 33°, and 35° 2 θ dominated by a broad amorphous hump centered ~22° 2 θ . The Li₆PON and Li₆SiPON pellets also show three peaks at 30°, 33°, and 35° 2 θ indexed to partially crystalline Li_{2.88}PN_{0.14}O_{3.73}. High Li⁺ content pellets seem to have higher intensity peaks compared to the pellets with lower Li⁺ concentrations as shown in Figure 1(b).

The absence of significant amounts of crystalline phases means XRD cannot be used to quantify phase compositions. Thus, XPS analyses were run on Li_xPON, LixSiPHN, Li_xSiPON pellets, Figure 1(c) reveals signature Li, P, O, Si, N peaks and minor peaks for C and Cl; the latter from residual NaCl. The carbon likely arises from brief air exposure forming Li₂CO₂.

Table 3 summarizes the XPS data. Li₃PON and Li₆PON conform to the XPS data reported previously. ^{9,45,48} XPS analyses also provide information about elemental bonding environments. The O 1s peak is attributed to Li-O-P, P-O-P, and P=O bonding environments as shown by the core-level spectrum presented in Figure S6. The Li/N ratios increase

Table 3. Atomic Ratios Based on XPS Analyses for Li_xPON, Li_xSiPHN, and Li_xSiPON

| ratio | Li ₃ PON | Li ₆ PON | Li ₂ SiPHN | Li ₃ SiPON | Li ₆ SiPON |
|-------|---------------------|---------------------|-----------------------|-----------------------|-----------------------|
| O/P | 6 | 4.5 | 3.15 | 3.56 | 5.54 |
| N/P | 1.25 | 1.66 | 1.84 | 1.9 | 2.4 |
| Li/N | 2.68 | 3.5 | 1.33 | 1.43 | 1.68 |

from ~2.7 to 3.5 as more LiNH₂ is added to the PON precursor. The experimental synthesis used had an N/P ratio of 3, the lower ratio found in the XPS suggests polymerization by loss of nitrogen. Quite important is the fact that the N/P ratio (1.25–1.66) is higher than the highest values reported for gas phase deposition techniques (0.92). APS further confirms that the Li₃PON and Li₆PON pellets have 4.7 and 5.35 at. % N, higher than atom% for Li_xPON films deposited by PE-MOCVD and RF magnetron sputtering (4 at. %).

The data indicate that the Li/N ratio increases from ~ 1.43 for Li₃SiPON to 1.68 for the Li₆SiPON precursor as more LiNH₂ is used. However, the ratio is smaller than calculated for Li₃PON (2.86) and Li₆PON (3.5) pellets, likely due to the silicon introduced. However, the N atom% for Li₃SiPON and Li₆SiPON are 8.5 and 6.7%, respectively. The N/P ratio (1.9–2.4) is still higher than found above for Li₃PON and Li₆PON. The presence of oxygen in the Li₂SiPHN precursor might be from brief air exposure during pellet pressing forming Li₂CO₃. The calculated atomic composition shows a Li/N ratio of 1.33 similar to Li₃SiPON in Table 3. However, this ratio is smaller than that introduced experimentally for Li₂SiPHN, likely a consequence of polymerization.

3.2. Ionic Conductivity of Polymer Electrolytes. Table 4 summarizes the total ambient conductivities of SS/Celgard

Table 4. Total Room Temperature Conductivity of Polymer Precursors

| conductivity (S/cm) |
|------------------------------|
| $1.1 \pm 0.3 \times 10^{-6}$ |
| $2.2 \pm 0.6 \times 10^{-6}$ |
| $2.7 \pm 0.4 \times 10^{-6}$ |
| $6.3 \pm 0.1 \times 10^{-6}$ |
| $8.8 \pm 0.4 \times 10^{-6}$ |
| |

+Li₃PON, Li₆PON, Li₂SiPHN, Li₃SiPON, and Li₆SiPON/SS. The polymers showed optimal Li⁺ diffusivity through the separator. The wet conductivities of electrolyte + Celgard are Li₃PON \ll Li₆PON \ll Li₂SiPHN \ll Li₃SiPON \ll Li₆SiPON. The incorporation of silicon into Li_xPON improves ionic conductivity (\sim 1 × 10⁻⁵S cm⁻¹) in good agreement with

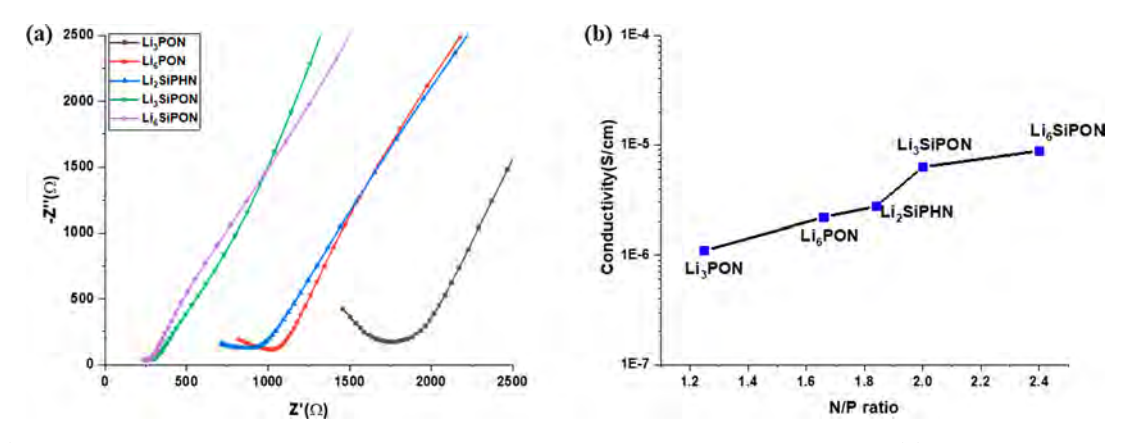


Figure 2. (a) Nyquist plots of SS/Celgard + Li, PON, Li, SiPHN, and Li, SiPON/SS at room temperature, (b) N/P ratio vs conductivity.

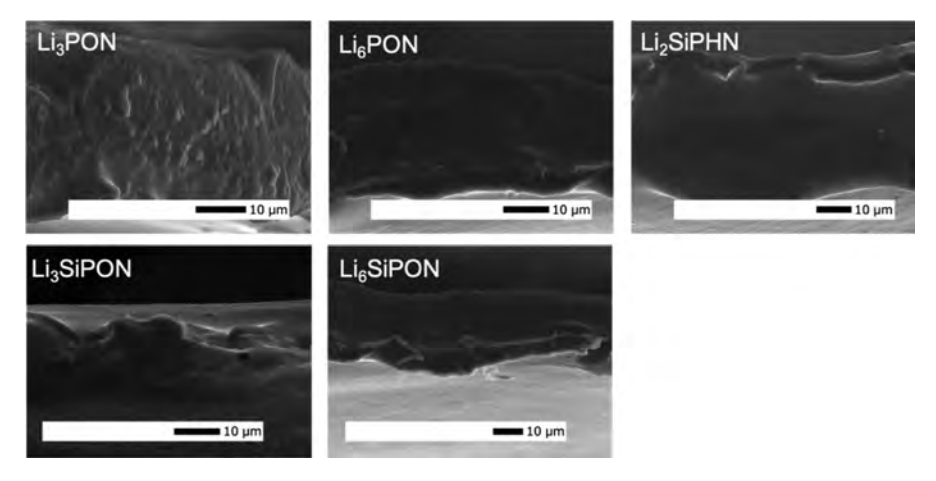


Figure 3. SEM fracture surface images Celgard + polymer precursors heated to 90 °C/12 h/Vacuum.

literature reports for Li_xSiPON thin films as shown in Figure 2(a). ^{27,28}

According to Roh et al. 1999, ⁴⁸ ionic conductivity is determined by the product of charge density and mobility. Hence, there are two ways to increase the Li⁺ ionic conductivity of Li_xPON emulated polymer electrolytes. One is to increase the Li⁺ content to increase charge carrier densities (i.e., Li₃PON to Li₆PON). This is difficult to achieve using gas phase deposition methods as Li content is nearly constant irrespective of the deposition technique (i.e., rf power). ⁵⁰ However, our synthesis route permits control of Li⁺ contents by varying LiNH₂ amounts.

The other is to change the inherent organization of the elements in the polymer to increase Li⁺ mobility (i.e., increasing the N/P ratio), again something difficult to do in gas phase approaches. Figure 2(b) shows the correlation of N/P ratio with polymer ionic conductivities. The increase in the N/P ratio results in a linear increase in conductivity for coated Celgard. A maximum conductivity of 8.8×10^{-6} S cm⁻¹ is achieved for the Li₆SiPON + Celgard polymer electrolyte with an N/P ratio of 2.4. Our N/P ratio is very high compared to traditional gas-phase techniques resulting in enhanced ionic conductivity. ^{45,50} The positive correlation between ionic conductivity and the N/P ratio can be attributed to the decrease in electrostatic energy as adding more $P-N < \frac{p}{P}$ cross-link structural units apparently increases Li⁺ mobility. ^{27,50}

In addition, aliovalent substitution of P⁵⁺ by Si⁴⁺ in Li_xPO₄ has been reported to create compositions that promote fast Li⁺ conduction by shortening the distance between Li⁺ binding

sites promoting superior ionic conductivity. The ionic conductivity of the LiSiPON has been reported to be superior to lithium silicophosphate, suggesting that introducing nitrogen to $\rm Li_2O-SiO_2-P_2O_5$ systems increases $\rm Li^+$ mobility presumably via reduced electrostatic interactions. Here we find that increasing the Si/P ratio also results in linear increases in conductivity deduced from the XPS at.% and EIS measurements for $\rm Li_xSiPHN$ and $\rm Li_xSiPON$ electrolytes, Figure S7 and Table S7. The Celgard+Li₆SiPON polymer electrolyte with a Si/P ratio of ~0.5 resulted in an ionic conductivity of 8.8×10^{-6} S cm $^{-1}$.

3.3. Morphology and Electrochemical Stability of Polymer Electrolytes. Figure 3 shows SEM fracture surface images of Celgard coated with polymer precursors. Celgard coated with polymer precursors did show interfaces. The coatings are optimal with average coating thicknesses of $5-10~\mu m$, see Table S8. The fracture surface images of the coatings reveal a uniform, smooth, and dense microstructure. Elemental map of the coating shows well-defined phosphorus, carbon, nitrogen, silicon, and chlorine distribution as shown in Figures S8 and S9.

Tolerance to high potential is very crucial for polymer electrolytes especially for development of long-life cycle ASBs with high energy densities. To obtain further insight concerning the electrochemical stability of the polymer electrolytes dissolved in THF, the linear sweep voltammograms were carried out at a scanning rate of 1 mV s $^{-1}$.

Figure 4 shows linear sweep voltammograms obtained for the Li/Celgard + polymer electrolytes/SS from 0 to 9 V. The

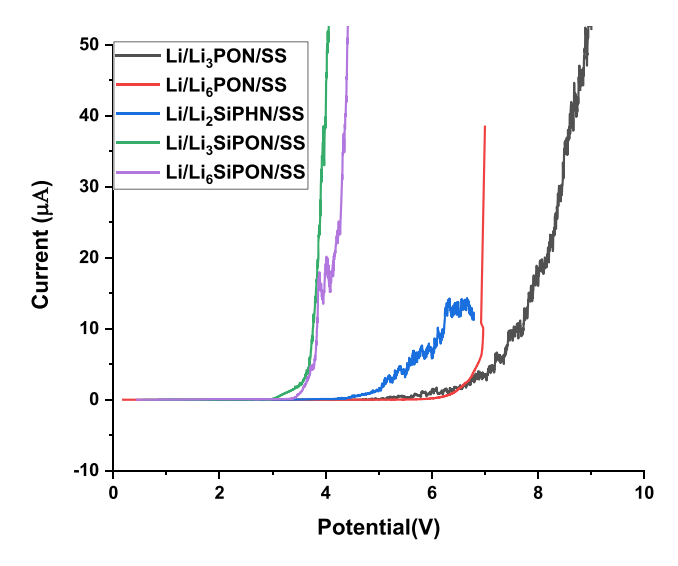


Figure 4. Linear sweep voltammograms of Li/Celgard + polymer precursor electrolytes/SS.

current increases dramatically when voltage exceeds 7 and 6 V for Li₃PON and Li₆PON polymer electrolytes respectively, indicating the decomposition potential of Li_xPON electrolyte in contact with Li. These values are higher than what is reported for gas phase deposited LiPON (0–5.0 V vs Li/Li⁺). These quite wide electrochemical stability windows appear suitable for Li ASBs with the high-potential cathode materials. 53

Comparatively, Li₂SiPHN shows a decomposition potential ~5 V, indicative of good oxidative stability for a polymer electrolyte based solely on phosphorus and nitrogen compared to the Li_xSiPON materials. Li₃SiPON and Li₆SiPON are only stable to 4 V which suggests a different decomposition potential perhaps due to the presence of Si. Thus, while incorporating Si enhances ionic conductivity by increasing the N/P ratio; it has a limited operating voltage window compared to the Li, PON electrolytes. The origin of the significant voltage difference depends on the electronegativity of the framework,⁵⁴ which weakens or strengthens the covalency of the Li-N bonds. The introduction of Si in the polymer precursors decreases the covalency of Li-N framework, which decreases the energy of the antibonding states. Hence, the difference in voltage stability between the Li+/Li couples in SiPON and PON framework.

3.4. Electrochemical Performance of Polymer Electrolytes. EIS was used to study the individual resistive elements that comprise the total Li/Celgard + polymer electrolyte/Li cell resistance. The symmetric cells were cycled at room temperature using DC cycling to determine the critical current densities.

3.4.1. Symmetric Cell Studies of Polymer Electrolytes. Figure 5(a) shows the Li/Celgard + Li₃PON/Li cell galvanostatically cycled at room temperature. The cell was tested for charge/discharge using a DC steady state method with a constant current density (± 0.05 mA cm⁻²). A stable potential of (± 0.007 V) was measured over the extended cycles. The Li/polymer precursor electrolyte interface stability was characterized vs current density. The potential vs capacity plot in Figure 5(b) shows that the Li₃PON electrolyte is stable to 0.5 mAh cm⁻².

Figure 5(c) shows a Li/Celgard + Li₃SiPON/Li cell galvanostatically cycled at ambient. The cell was tested for charge/discharge using a constant current ($\pm 0.15-0.75$ mA). The symmetric cell shows a stable voltage response (0.04 V) when a high current density of 0.75 mA is used. The potential vs capacity plot in Figure 5(d) also shows that the electrolyte is stable to 0.375 mAh cm⁻² without showing any voltage fluctuation or polarization.

Figure 5(e) and (d) shows the selected overpotential profiles of subsequent lithium plating/stripping process on the working electrode in the Li/Li symmetrical cells with Celgard + Li₃SiPON as the electrolyte. At current density ($j = 0.1 \text{ mA/cm}^2$), there is a heterogeneous lithium dissolution region on/at the lithium metal anode. The overall dissolution process in Figure 5(e) and (d) is divided into four parts (a, b, c, and d). In the first part (a), the lithium dissolution process starts with an immediate steeply increase in the potential to $(0.1 \text{ V at } j = 0.1 \text{ mA/cm}^2)$ which is the maximum overpotential in the whole experiment, whereas the second part shows a decrease of the overpotential (b), and followed by a fast drop to 0.03 V (c). The dissolution process shows further decreases in potential to 0.02 V (d).

The rapid increase of the overpotential indicates the end of the corresponding dissolution process. The overpotential is high in region (a) because the process primarily takes place on the pristine, smooth, and low surface area Li substrate. The decrease of the overpotential after the first cycle confirms that the corresponding lithium dissolution mostly takes place form an already roughened Li surface. Similar to dendrite formation, Li plating and stripping also change the surface morphology of the electrode. The increase in current distribution ($j = 0.6 \text{ mA/cm}^2$) might lead to the crack of the SEI and increase in the electrode surface area and decrease of the SEI resistance (e). As the local roughness makes spots that are preferable for Li stripping and deposition, continuous cycling will result in a decrease in overpotential (f) for the rest of the cycle.

The Celgard coated with $\rm Li_6 PON$ polymer show unstable voltage spikes at 0.1 mA current density, Figure S10. Higher current densities (>0.1 mA) seem to result in higher interfacial impedance as seen by the increases in voltage response to 1 V. However, the symmetric cell shows a stable voltage response (0.25 V) when at 0.075 mA, Figure 6(a). The potential vs capacity plot in Figure 6(b) shows that the electrolyte is stable to 0.375 mAh cm⁻².

Celgard coated with Li₆SiPON shows an ideal voltage response suggesting that there was a minimum interfacial impedance throughout the galvanostatic cycling at room temperature as shown in Figure 6(c). This is revealed by a low voltage response at higher current densities ($\pm 1.5-7.5$ mA). The interfacial impedance is nearly constant when the current density increases to (± 7.5 mA) demonstrating by the voltage response and confirmed per Ohms' law (R = V/I). The potential vs capacity plot shows that the electrolyte is stable to 3.5 mAh cm⁻². These high current densities are attributed to the stability of the Li₆SiPON polymer electrolyte against Li metal with very low ohmic resistivity of ~ 1 Ω . In addition, the high critical current density of the polymer electrolyte matches rate performances of state-of-art Li⁺ at 1–3 mA cm^{-2,56}

Figure S11(a) shows Li/Celgard + Li₂SiPHN/Li cells galvanostatically cycled at room temperature. The cell was tested for charge and discharge using a DC steady-state method in which a constant current (± 7.5 mA) was used. The

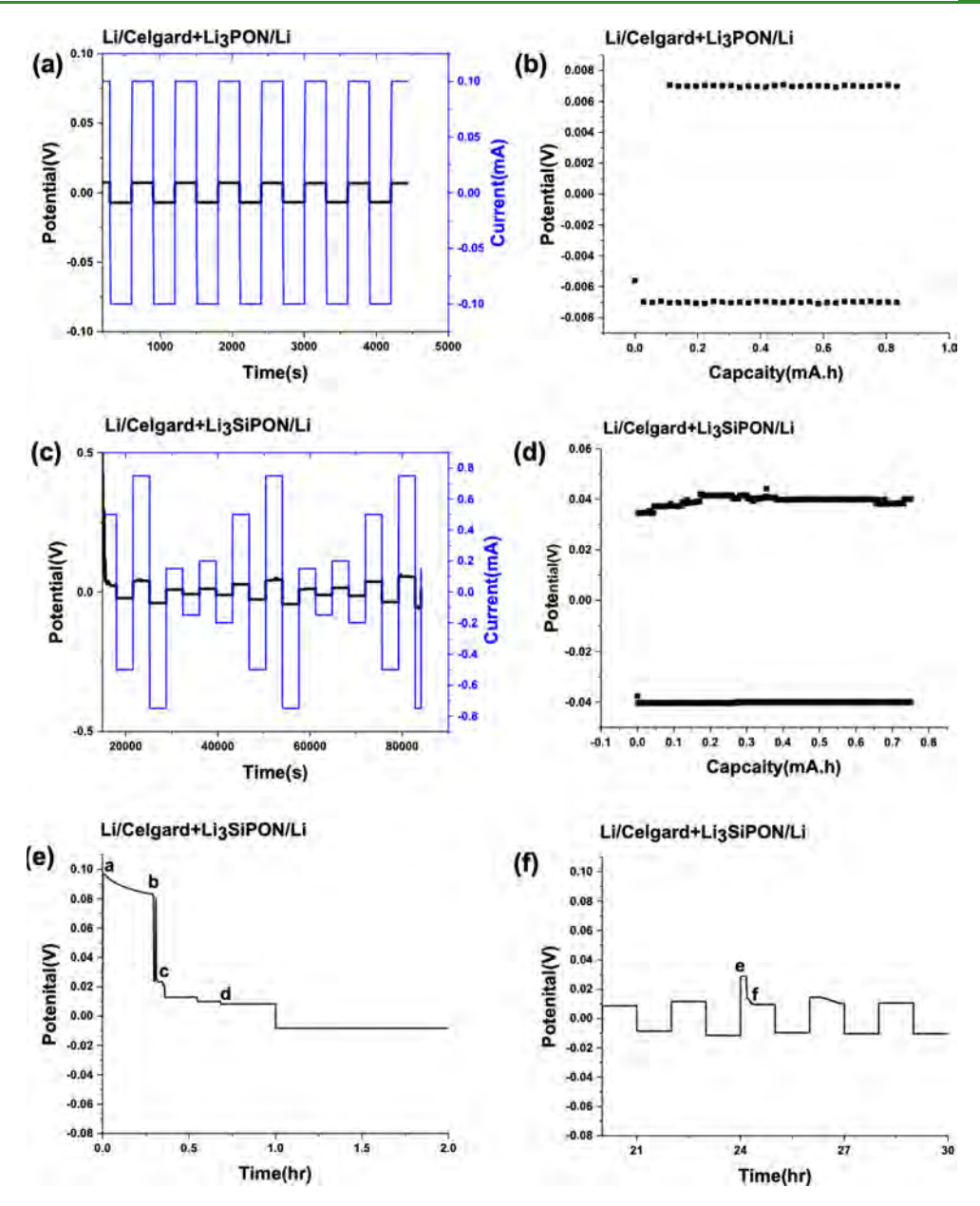


Figure 5. Galvanostatic cycling of Li/Celgard + Li₃PON (a, b) and Li₃SiPON (c, d) /Li symmetric cell at the current density of ± 0.1 mA. Selected overpotential profiles of Li/Celgard + Li₃SiPON/Li symmetric cell at the current densities of ± 0.13 mA/cm² (e) and 0.66 mA/cm²(f).

symmetric cell shows a voltage response (0.02 V) for the first 20 h at a constant current density of 7.5 mA. The overpotential gradually increases to \sim 0.025 V after the first 10 cycles. This indicates a general increase in the overall resistance vs lithium deposition. Long-term cycling shows that the overpotential (\sim 0.03 V) profile becomes constant after the first 20 initial cycles. The potential vs capacity plot also shows that the Li₂SiPHN electrolyte is stable up to 3.75 mAh cm⁻² as shown in Figure S11(b).

3.4.2. Transference Number Studies of Polymer Electrolytes. Figure 7 shows the Nyquist plots of Li/Celgard + polymer precursor/Li symmetric cells at room temperature before cycling. The equivalent circuit is shown in Figure S12. R_1 and R_2 correspond to the Ohmic resistance of the polymer electrolyte and the electrode surface resistance, referred to as $(R_{\rm SEI})$. The R_3 in the inset of Figure S12 refers to charge transfer resistance.

EIS measurements compare the impedance differences of the symmetric cells using the different polymer electrolytes. In general, the high-frequency semicircle relates to Li⁺ migration resistance through the polymer electrolyte interface, and the lower frequency semicircle relates to charge transfer resistance ($R_{\rm ct}$). The low frequency semicircle diameter was divided by a factor of 2 to determine the $R_{\rm ct}$ as the cell employed two Li metals of equal area. At room temperature, a $R_{\rm ct}$ of $\sim\!50~\Omega$ cm² was measured for Li₂SiPHN polymer electrolyte. This $R_{\rm ct}$ value is similar to state-of-art Li⁺ liquid electrolytes, typically tens of Ω cm². The Nyquist plots mainly show high resistance at the electrode surface, suggesting that the overpotential of Li stripping and plating processes are dominated by the nature of SEI at the Li/electrolyte interface.

Lithium transference number $(t_{\rm Li}^+)$ was determined following the procedure and equation suggested by Bruce et al. Symmetrical cells using (Li/polymer coated Celgard electrolytes/Li) were monitored under chronoamperometry

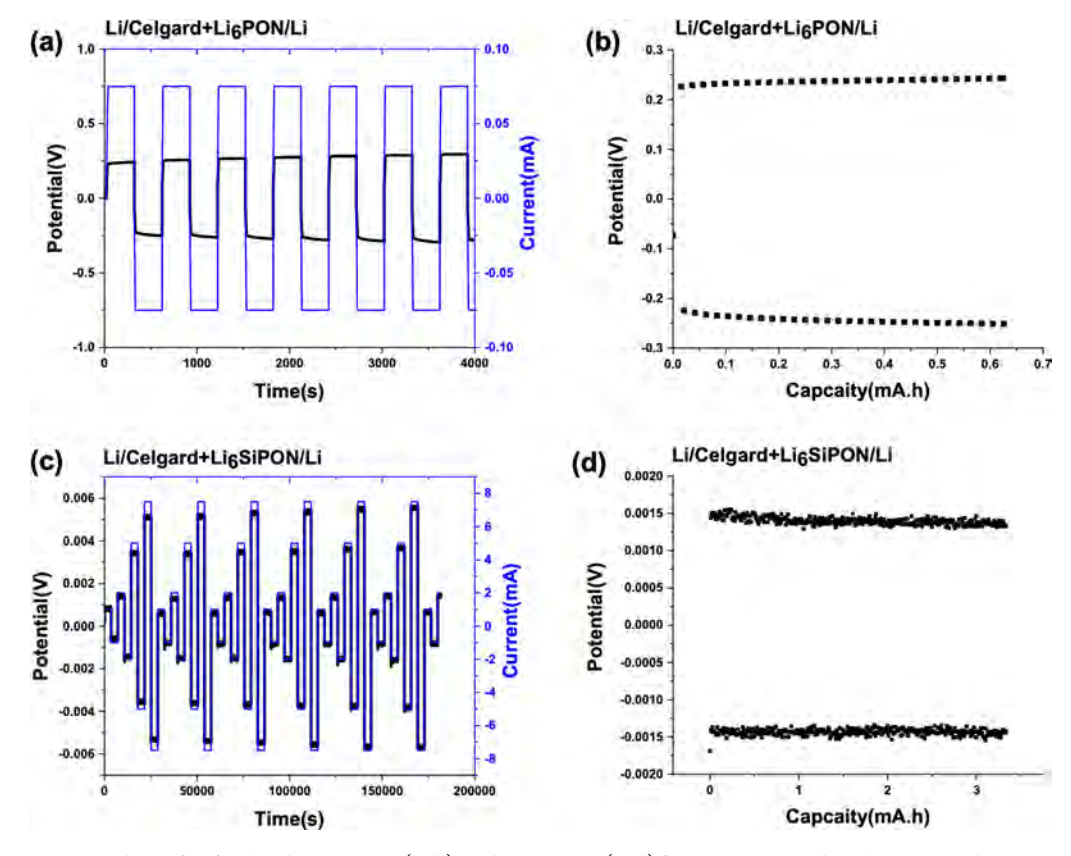


Figure 6. Galvanostatic cycling of Li/Celgard + Li₆PON (a, b) and Li₆SiPON (c, d)/Li symmetric cell at the current densities of $\pm 0.1-7.5$ mA. The blue line corresponds to the constant current and the black line is the voltage response.

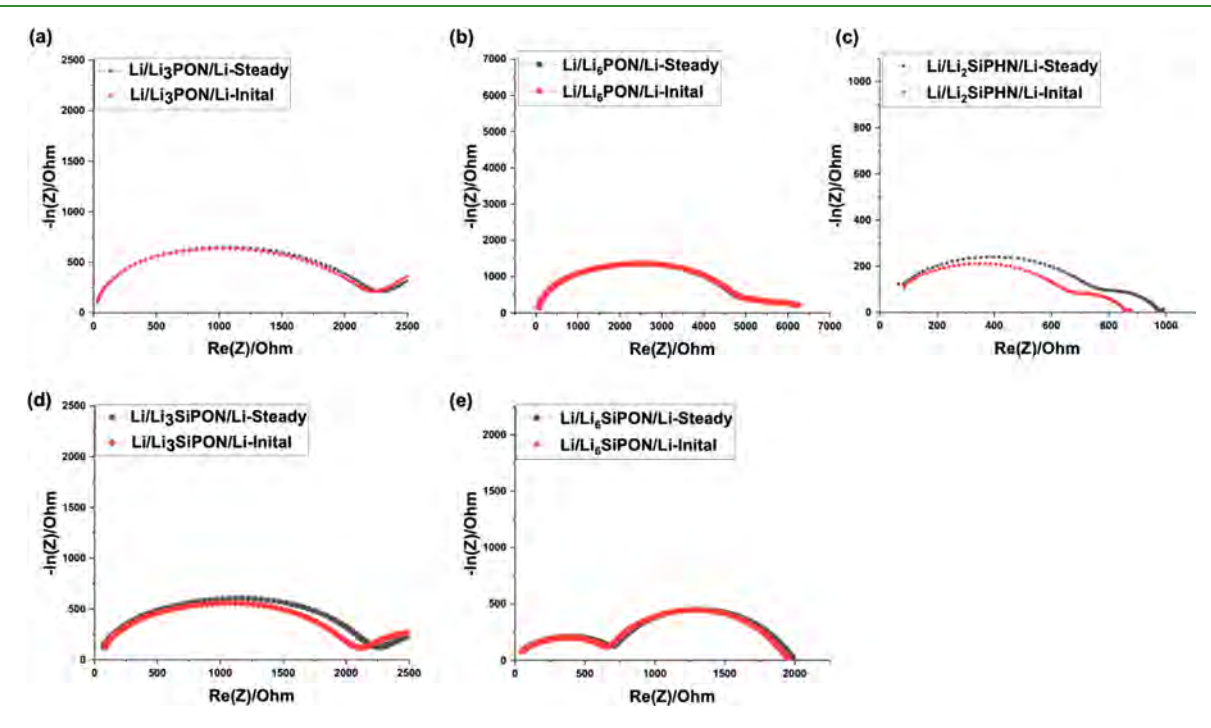


Figure 7. Nyquist plots of Li/Celgard+ (a) Li₃PON, (b) Li₆PON, (c) Li₂SiPHN, (d) Li₃SiPON, and (e) Li₆SiPON/Li cells.

until a steady-state current was reached. The initial (I_0) and steady-state (I_{SS}) currents in addition to the initial (Z_0) and steady-state (Z_{SS}) resistances were obtained from the chronoamperometry and EIS measurements. Transference number (t_{Li}^+) was calculated using the following equation:

$${t_{\mathrm{Li}}}^+ = I_{\mathrm{SS}}(\mathrm{DV} - Z_0 \times I_0) / I_0(\mathrm{DV} - Z_{\mathrm{SS}} \times I_{\mathrm{SS}})$$

The stability of polymer electrolyte against Li was evaluated by monitoring the electrochemical impedance spectra of Li/ polymer coated Celgard electrolytes/Li symmetrical cell before and after chronoamperometry measurements under open circuit conditions at ambient.

Figure 7 shows Nyquist plots of symmetric cells assembled with polymer precursor coated Celgard electrolytes. The Nyquist plots for cells assembled with Li₆PON and Li₆SiPON electrolytes show that the impedance is stable before and after steady-state current. However, the impedance increased after steady-state current was achieved for cells assembled with Li₂SiPHN and Li₃SiPON polymer electrolytes. The spectra start with the Ohmic resistance and then show a semicircle at lower frequencies. The Ohmic part of the cell resistance is determined by the ionic conductivity of the polymer electrolytes, the following semicircle consequently corresponds to the capacitive properties, SEI, and charge-transfer resistance at the Li electrodes. Since both plots start at the same high frequency (Ohmic part), the ionic conductivity of the Li₂SiPHN and Li₀SiPON precursors are the same before and after steady-state current measurement, hence the increment in impedance has to be related to the formation of SEI and charge-transfer resistance at the Li electrodes.

Interfacial resistance (Z_0 and Z_{ss}) values were obtained by analyzing the real resistances of the semicircle of EIS Nyquist plots. After 1 h, a steady-state current was achieved. Figure S13 shows chronoamperometry plots of symmetric cells assembled with polymer precursor coated Celgard electrolytes. The increase in the transference number for the polymer electrolyte is indicative of a chemical interaction between Li and PON and SiPON, that in turn afforded high Li⁺ mobility. It is noteworthy that since the interfacial resistances were higher than the electrolyte resistance, this steady-state method is now considered less of a quantitative and more of a qualitative comparison of the increase in tLi⁺.

Table 5 lists the average transference numbers of polymer precursor coated Celgards assembled in symmetric cell

Table 5. Calculated Li⁺ Transfer Numbers of Polymer Precursor Coated Celgard Electrolytes

| electrolyte | <i>t</i> Li ⁺ avg |
|-----------------------|------------------------------|
| Li ₃ PON | 0.8 ± 0.2 |
| Li ₆ PON | 0.8 ± 0.6 |
| Li ₂ SiPHN | 0.9 ± 0.2 |
| Li ₃ SiPON | 0.8 ± 0.3 |
| Li ₆ SiPON | 0.7 ± 0.6 |
| | |

configuration. The Li₂SiPHN precursor showed an ideal transference number of $\sim\!\!0.9$ comparable to solid-state electrolytes. From these preliminary results, the transference number is in the order of Li₆SiPON < Li₃PON < Li₃SiPON < Li₆PON < Li₂SiPHN.

3.4.3. Electrical Conductivity of Polymer Electrolytes. The electronic conductivity of the polymer electrolytes was determined by DC measurements of the current under

potential polarization using Bio-Logic SP 300 potentiostat with low current functions (current resolution <1 nA). The potential was ramped in the range of -0.03 to +0.03 V with a step of 10 mV and was held at each step for up to 1 h. The stabilized current at each step was used to determine the electronic conductivity. The electronic conductivity is deduced from the stabilized current (I_{ss}) using the relation:

$$\sigma_{\alpha} = (t \times I_{ss})/(A \times U)$$

where t is the thickness of the Celgard (25 μ m), A is the area of the Li electrode (radius = 8 mm), and U is the applied voltage.

The electronic conductivities of Celgard coated with Li_xPON polymer precursors measured by DC polarization experiments are summarized in Table 6. Representative current—voltage plots of Li_3PON and Li_6PON are shown in Figures 8(a, b) and 8(c, d), respectively. The stabilized current shows a linear increase with the step increase of voltage as expected from Ohms law (V = IR). The Li_3PON and Li_6PON polymer electrolytes showed an average electrical conductivity of $\sim 3 \times 10^{-10}$ and 2.6×10^{-10} S/cm, respectively. These values are higher than what is reported for Li_xPON systems ($10^{-15} - 10^{-12}$ S/cm). S8,59 However, the reported electrical conductivities are much lower than LLZO ($10^{-8} - 10^{-7}\text{S/cm}$) and $\text{Li}_2\text{S} - \text{P}_2\text{S}_5$ ($10^{-9} - 10^{-8}\text{S/cm}$) solid electrolytes. It is also worth noting that the electrical conductivity measurements are done on the polymer precursor coated separators, the precursor by itself might have lower electronic conductivity.

The electronic conductivities of Li₂SiPON and Li₂SiPHN polymer precursors coated Celgards are measured by DC polarization experiments and are summarized in Table 6. Representative current-voltage plots of Li₂SiPHN and Li_xSiPON are shown in Figures S14 and 9, respectively. The Li₂SiPHN polymer electrolytes showed an average electrical conductivity of $\sim 2.7 \times 10^{-9}$ S/cm. Whereas, the Li₃SiPON and Li₆SiPON polymer electrolytes showed lower average electronic conductivities of $\sim 6.2 \times 10^{-10}$ and 1.8×10^{-10} S/ cm, respectively. The increase in Li+ concentration from Li₃SiPON to Li₆SiPON seems to decrease the electrical conductivity in Li₆SiPON polymer coated Celgard electrolytes. Similar phenomena are observed when the Li concentration increased from Li₃PON to Li₆PON as shown in Figure 8. Further studies about the space charge region and heterojunction between the Li metal and the polymer precursor electrolytes are needed to understand the electrical conductivity of the electrolyte.

Interestingly, the Celgard coated with Li₆SiPON polymer precursor showed the lowest electrical conductivity when compared to the other polymer electrolytes. This electrolyte also showed the highest ionic conductivity and high critical current density (3.75 mA cm⁻²). All of these properties

Table 6. List of Electrical Conductivities for Li/Celgard + Polymer Precursor/Li Cell Obtained by DC Measurements

| potential (mV) | Li ₃ PON $\sigma_{\rm e}$ (S/cm) | $\text{Li}_6\text{PON }\sigma_{\text{e}}\ (\text{S/cm})$ | Li ₂ SiPHN $\sigma_{\rm e}$ (S/cm) | Li ₃ SiPON $\sigma_{\rm e}$ (S/cm) | Li ₆ SiPON $\sigma_{\rm e}$ (S/cm) |
|----------------|---|--|---|---|---|
| -30 | 2.9×10^{-10} | 2.6×10^{-10} | 2.5×10^{-9} | 6.2×10^{-10} | 1.9×10^{-10} |
| -20 | 2.9×10^{-10} | 2.7×10^{-10} | 2.5×10^{-9} | 6.2×10^{-10} | 1.9×10^{-10} |
| -10 | 2.7×10^{-10} | 2.5×10^{-10} | 2.5×10^{-9} | 6.2×10^{-10} | 1.9×10^{-10} |
| 10 | 3.1×10^{-10} | 2.5×10^{-10} | 2.5×10^{-9} | 6.2×10^{-10} | 1.7×10^{-10} |
| 20 | 3.1×10^{-10} | 2.7×10^{-10} | 3.0×10^{-9} | 6.2×10^{-10} | 1.7×10^{-10} |
| 30 | 3.0×10^{-10} | 2.6×10^{-10} | 3.3×10^{-9} | 6.2×10^{-10} | 1.7×10^{-10} |

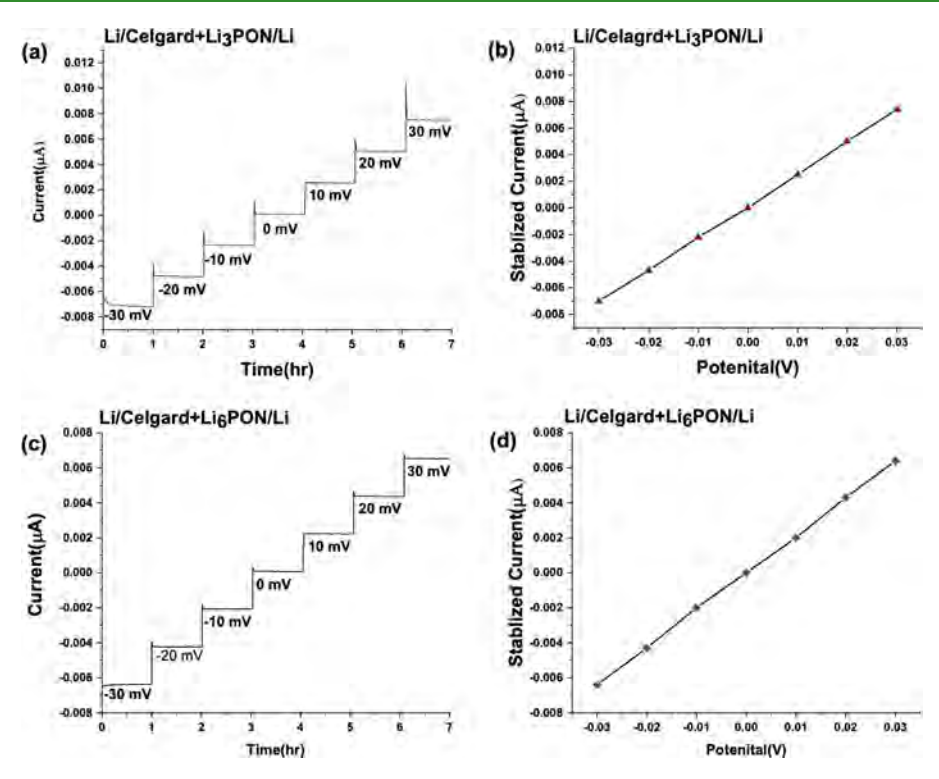


Figure 8. Time dependence of current during step voltages (a and c). Stabilized current-voltage relations of Li/Li_xPON/Li cells (b and d).

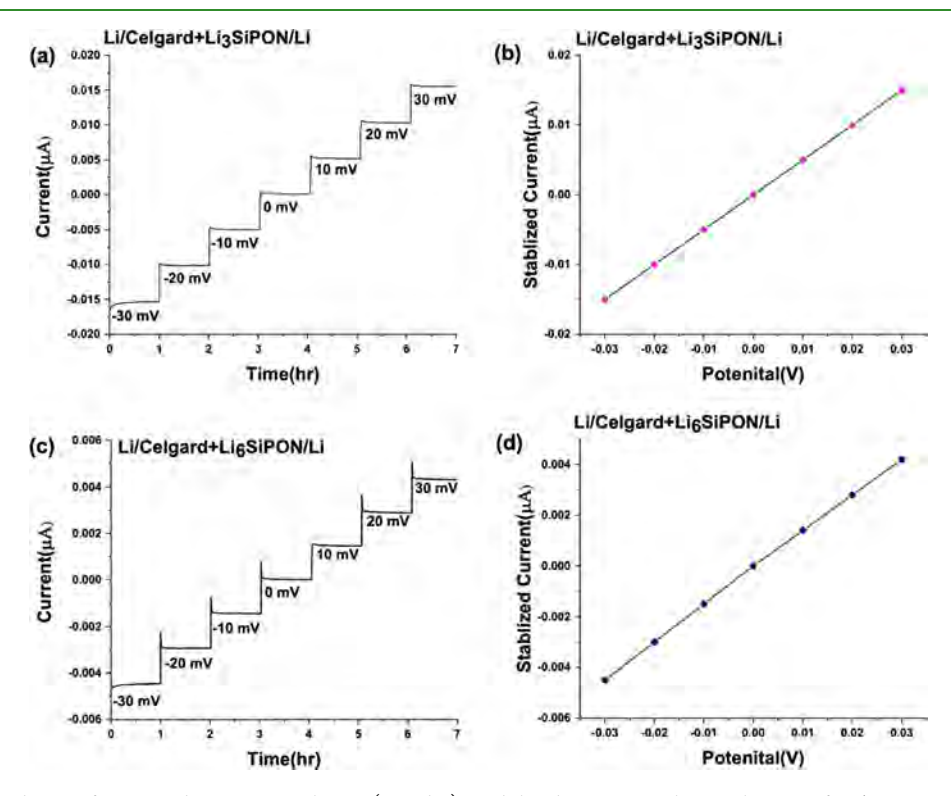


Figure 9. Time dependence of current during step voltages (a and c). Stabilized current–voltage relations of Li/Li_xSiPON/Li cells (b and d).

ensured that Li₆SiPON has a similar dendrite suppression capability to that of Li_{*}PON.

The Li₆SiPON polymer precursor electrolyte was used to assemble a half cell with Li metal and SPAN cathode. Detailed synthesis and performance of SPAN cathodes can be found elsewhere.³⁰ Figure 10 shows the results of SPAN/Celgard + Li₆SiPON/Li cells cycled at 0.5 C rates. The Li-SPAN battery

cycled for 220 h. without any polarization or voltage fluctuation. The half-cell was cycled from 1 to 3 V for 122 cycles. The half-cell showed an initial capacity ~ 1500 mAh $g_{\rm sulfur}^{-1}$; 90% of theory for Li–S batteries. The capacity decreases to 1000 mAh $g_{\rm sulfur}^{-1}$ after the 40th cycle and gradually to 750 mAh $g_{\rm sulfur}^{-1}$ thereafter. The reported capacity

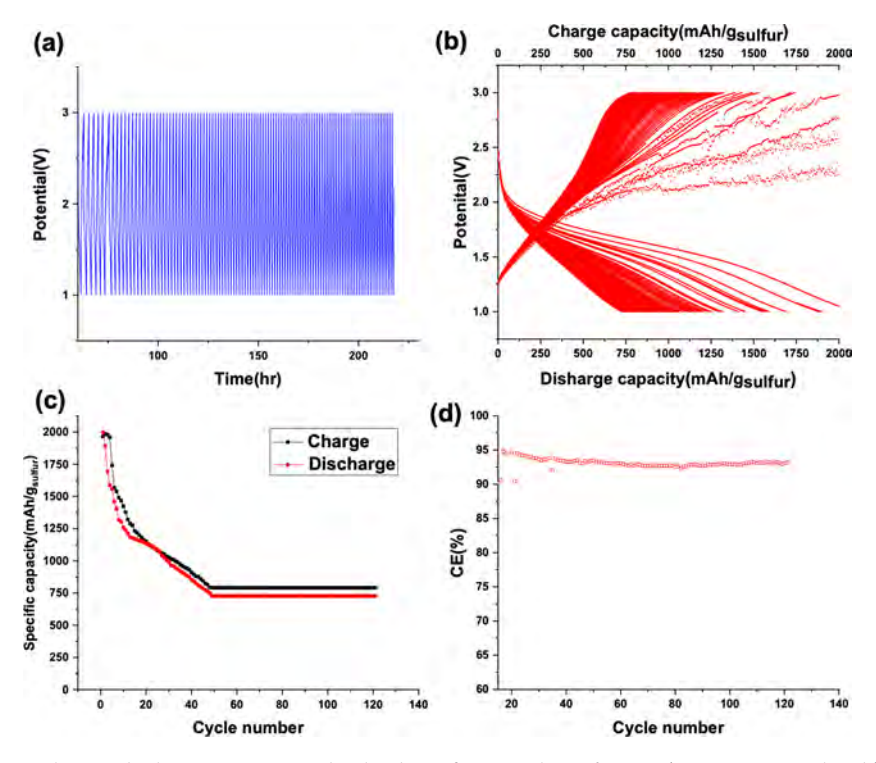


Figure 10. Potential vs time, charge-discharge capacity, and columbic efficiency plots of SPAN/Li₆SiPON + Celgard/Li at 0.5 C.

Table 7. Comparison of Reported Polymer Electrolytes for Li-S Batteries

| electrolyte | retained capacity | C-rate | Columbic efficiency | ref |
|---|-------------------|--------|---------------------|-----------|
| 1 M LITFSI/DOL/DME/PYR ₁₄ TFSI | 846 | 0.2 | 94.2 | 63 |
| Li[TFSA]/G4/HFE | 600 | 0.5 | 98 | 64 |
| $[Li(G4)_1][TFSA]$ | 450 | 0.5 | 98 | |
| 1 M LiTFSI/DOL/DME | 815 | 0.5 | 91.3 | 65 |
| PEO at 104 °C | 200 | 0.1 | | 66 |
| PEGDME at 23 °C | 100 | 0.05 | N/A | |
| PEMO at 60 °C | 50 | 0.025 | | |
| Li ₆ SiPON at 23 °C | 750 | 0.5 | 92 | this work |

is much improved when compared to Li-S batteries assembled with polymer electrolytes as listed in Table 7.

The $\rm Li_6SiPON$ polymer electrolyte shows high electrochemical stability at 0.5 C for 122 cycles. The half-cell shows a slight decrease from 95% to 92% efficiency after the first 40 cycles. It remains ~92% thereafter. The stability and high performance of the nearly all solid-state battery can be ascribed to the unique performance of SPAN and the polymer electrolyte. The most important feature of SPAN is that the sulfur is covalently bound to a polyaromatic backbone and forms different structural motifs that reduce detrimental polysulfide dissolution. 30,62

A high rate of capacity fade is observed for the Li-S battery with polymer electrolytes. Three plausible explanations may be given. One is the irreversibility of some of the polysulfide reactions. Another is the diffusion of polysulfides into the electrolyte. A third is the loss of electrical contact during cycling. The last factor might be due to several phenomena, including the formation of large particles of highly resistive sulfur or lithium sulfide, the migration of polysulfides away from the carbon phase, and the agglomeration of sulfur or carbon particles as a result of the pressure exerted on the cell. Since the SPAN cathode can eliminate the formation of polysulfides that results in a fast capacity loss, future work will

rely on the optimization of the electrical contact between the SPAN cathode and the polymer precursor electrolytes. The poor electrical contact is ascribed to result in a decrease in columbic efficiency. Efforts to optimize the critical current densities of the other polymer electrolytes and for assembly of ASBs remains future work. The interfacial behavior directly dictates the lifespan, energy density, and safety of all solid-state batteries. We believe that these polymer electrolytes might lower the interfacial resistance and stabilize the interfacial performance of all solid-state batteries.

4. CONCLUSIONS

In summary, we have presented the synthesis of a set of polymers that emulate LiPON chemistries and that allow simple and extensive control of composition, degree of lithiation, and incorporation of silicon as well as exclusion of oxygen and understand their effects on the ionic conductivity. We will demonstrate in the future their use in generating Li_xPON , Li_xSiPON , and Li_xSiPHN glasses. The intent was to find a simple alternative to the equipment and energy intensive gas phase deposition methods. Our approach involves the synthesis of $O=P(\text{NH}_2)_3$ from $OPCl_3$ followed by lithiation with LiNH_2 .

The ionic conductivity of the polymer electrolytes increases with increasing amounts of Li and optimizing the N/P ratio. Maximum ambient ionic conductivities of $\sim 1 \times 10^{-5} \mathrm{S} \ \mathrm{cm}^{-1}$ are achieved for the Li₆SiPON with 2.4 N/P ratio. The polymer electrolytes also show high ohmic stability against Li metal at current densities of 0.375–3.75 mAh cm⁻². In addition, the Li₂SiPHN precursor showed an ideal transference number of ~ 0.9 comparable to solid-state electrolytes. Furthermore, the Li₆SiPON polymer electrolyte was used to assemble a nearly all solid-state Li/SPAN battery. The stability and high performance of the half-cell was attributed to the unique performance of the SPAN and the polymer electrolyte.

ASSOCIATED CONTENT

Supporting Information

The Supporting Information is available free of charge at https://pubs.acs.org/doi/10.1021/acsami.0c03341.

Analytical methods and basic characterization of the polymer precursors (PDF)

AUTHOR INFORMATION

Corresponding Author

Richard M. Laine — Materials Science and Engineering, University of Michigan, Ann Arbor, Michigan 48109, United States; oorcid.org/0000-0003-4939-3514; Phone: +1 734 764-6203; Email: talsdad@umich.edu

Authors

Eleni Temeche — Materials Science and Engineering, University of Michigan, Ann Arbor, Michigan 48109, United States Xinyu Zhang — Materials Science and Engineering, University of Michigan, Ann Arbor, Michigan 48109, United States

Complete contact information is available at: https://pubs.acs.org/10.1021/acsami.0c03341

Author Contributions

The manuscript was written through contributions of all authors. All authors have given approval to the final version of the manuscript.

Funding

DOE through Batt500 Seedling project DE-EE0008235, Daimler Mercedes, and DMR NSF Grant No. DMR 099217.

Notes

The authors declare no competing financial interest.

ACKNOWLEDGMENTS

We are grateful for the support of a significant portion of this work by DOE through Batt500 Seedling project DE-EE0008235 and a gift from Daimler Mercedes. A portion of this work was also supported by a DMR NSF Grant No. DMR 099217. We also thank the University of Michigan Energy Institute (UMEI) and Michigan Translational Research and Commercialization (MTRAC) program for support of the purchase chemicals, solvents, and furnace. We like to thank Mercedes-Benz Research & Development North America (MBRDNA) for their support. We especially thank Mr. Tobias Glossman and Professor Dr. Andreas Hintennach of Mercedes-Daimler for their encouragement. We also thank Mr. Andrew Alexander for his assistant in providing the computer program for polymer precursor structure calculations based MALDI-ToF.

REFERENCES

- (1) Put, B.; Vereecken, P. M.; Meersschaut, J.; Sepúlveda, A.; Stesmans, A. Electrical Characterization of Ultrathin RF-Sputtered LiPON Layers for Nanoscale Batteries. *ACS Appl. Mater. Interfaces* **2016**, *8*, 7060–7069.
- (2) Oudenhoven, J. F. M.; Baggetto, L.; Notten, P. H. L. All-Solid-State Lithium-Ion Microbatteries: A Review of Various Three-Dimensional Concepts. *Adv. Energy Mater.* **2011**, *1*, 10–33.
- (3) Zhang, H.; Yu, X.; Braun, P. V. Three-Dimensional Bicontinuous Ultrafast-Charge and-Discharge Bulk Battery Electrodes. *Nat. Nanotechnol.* **2011**, *6*, 277–281.
- (4) Vereecken, P. M.; Huyghebaert, C. Conformal Deposition for 3D Thin-Film Batteries. *ECS Trans.* **2013**, *58*, 111–118.
- (5) Rubloff, G. W.; Kozen, A. C.; Bok Lee, S. From Nanoscience to Solutions in Electrochemical Energy Storage. *J. Vac. Sci. Technol., A* **2013**, *31*, 058503.
- (6) Bates, J. B.; Dudney, N. J.; Gruzalski, G. R.; Zuhr, R. A.; Choudhury, A.; Luck, C. F.; Robertson, J. D. Electrical Properties of Amorphous Lithium Electrolyte Thin Films. *Solid State Ionics* **1992**, 53, 647–654.
- (7) Wang, B.; Kwak, B. S.; Sales, B. C.; Bates, J. B. Ionic Conductivities and Structure of Lithium Phosphorus Oxynitride Glasses. *J. Non-Cryst. Solids* **1995**, *183*, 297–306.
- (8) Yu, X.; Bates, J. B.; Jellison, G. E.; Hart, F. X. A Stable Thin-Film Lithium Electrolyte: Lithium Phosphorus Oxynitride. *J. Electrochem. Soc.* 1997, 144, 524–532.
- (9) Bates, J. B.; Dudney, N. J.; Gruzalski, G. R.; Zuhr, R. A.; Choudhury, A.; Luck, C. F.; Robertson, J. D. Fabrication and Characterization of Amorphous Lithium Electrolyte Thin Films and Rechargeable Thin-Film Batteries. *J. Power Sources* **1993**, *43*, 103–110.
- (10) Reyes Jiménez, A.; Nölle, R.; Wagner, R.; Hüsker, J.; Kolek, M.; Schmuch, R.; Winter, M.; Placke, T. A Step towards Understanding the Beneficial Influence of a LIPON-Based Artificial SEI on Silicon Thin Film Anodes in Lithium-Ion Batteries. *Nanoscale* **2018**, *10*, 2128–2137.
- (11) Nimisha, C. S.; Rao, K. Y.; Venkatesh, G.; Rao, G. M.; Munichandraiah, N. Sputter Deposited LiPON Thin Films from Powder Target as Electrolyte for Thin Film Battery Applications. *Thin Solid Films* **2011**, *519*, 3401–3406.
- (12) Hamon, Y.; Douard, A.; Sabary, F.; Marcel, C.; Vinatier, P.; Pecquenard, B.; Levasseur, A. Influence of Sputtering Conditions on Ionic Conductivity of LiPON Thin Films. *Solid State Ionics* **2006**, *177*, 257–261.
- (13) Zhao, S.; Fu, Z.; Qin, Q. A Solid-State Electrolyte Lithium Phosphorus Oxynitride Film Prepared by Pulsed Laser Deposition. *Thin Solid Films* **2002**, *415*, 108–113.
- (14) Liu, W. Y.; Fu, Z. W.; Li, C. L.; Qin, Q. Z. Lithium Phosphorus Oxynitride Thin Film Fabricated by a Nitrogen Plasma-Assisted Deposition of E-Beam Reaction Evaporation. *Electrochem. Solid-State Lett.* **2004**, *7*, J36–J40.
- (15) Vereda, F.; Goldner, R. B.; Haas, T. E.; Zerigian, P. Rapidly Grown IBAD LiPON Films with High Li-Ion Conductivity and Electrochemical Stability. *Electrochem. Solid-State Lett.* **2002**, *5* (11), A239–A241.
- (16) Kim, Y. G.; Wadley, H. N. G. Lithium Phosphorous Oxynitride Films Synthesized by a Plasma-Assisted Directed Vapor Deposition Approach. *J. Vac. Sci. Technol., A* **2008**, *26*, 174.
- (17) Nowak, S.; Berkemeier, F.; Schmitz, G. Ultra-Thin LiPON Films Fundamental Properties and Application in Solid State Thin Film Model Batteries. *J. Power Sources* **2015**, *275*, 144–150.
- (18) Kim, H. T.; Mun, T.; Park, C.; Jin, S. W.; Park, H. Y. Characteristics of Lithium Phosphorous Oxynitride Thin Films Deposited by Metal-Organic Chemical Vapor Deposition Technique. *J. Power Sources* **2013**, 244, 641–645.
- (19) Ruzmetov, D.; Oleshko, V. P.; Haney, P. M.; Lezec, H. J.; Karki, K.; Baloch, K. H.; Agrawal, A. K.; Davydov, A. V.; Krylyuk, S.; Liu, Y.; Huang, J.; Tanase, M.; Cumings, J.; Talin, A. A. Electrolyte Stability

- Determines Scaling Limits for Solid-State 3D Li Ion Batteries. *Nano Lett.* **2012**, *12* (1), 505511.
- (20) Xu, F.; Dudney, N. J.; Veith, G. M.; Kim, Y.; Erdonmez, C.; Lai, W.; Chiang, Y. M. Properties of Lithium Phosphorus Oxynitride (Lipon) for 3D Solid-State Lithium Batteries. *J. Mater. Res.* **2010**, 25 (8), 1507–1515.
- (21) Kozen, A. C.; Pearse, A. J.; Lin, C. F.; Noked, M.; Rubloff, G. W. Atomic Layer Deposition of the Solid Electrolyte LiPON. *Chem. Mater.* **2015**, 27 (15), 5324–5331.
- (22) Laine, R. M.; Babonneau, F. Preceramic Polymer Routes to Silicon Carbide. *Chem. Mater.* **1993**, *5*, 260–279.
- (23) Yi, E.; Temeche, E.; Laine, R. M. Superionically Conducting B"-Al₂O₃ Thin Films Processed Using Flame Synthesized Nanopowders. *J. Mater. Chem. A* **2018**, *6*, 12411–12419.
- (24) Okamura, K. Ceramic Fibres from Polymer Precursors. Composites 1987, 18 (2), 107–120.
- (25) Bill, J.; Aldinger, F. Precursor-Derived Covalent Ceramics. In Precursor-Derived Ceramics: Synthesis, Structures and High Temperature Mechanical Properties; 2008 DOI: 10.1002/9783527613823.ch4.
- (26) Greil, P. Polymer Derived Engineering Ceramics. Adv. Eng. Mater. 2000, 2 (6), 339–348.
- (27) Lee, S. J.; Bae, J. H.; Lee, H. W.; Baik, H. K.; Lee, S. M. Electrical Conductivity in Li-Si-P-O-N Oxynitride Thin-Films. *J. Power Sources* **2003**, *123* (1), 61–64.
- (28) Lee, S. J.; Baik, H. K.; Lee, S. M. An All-Solid-State Thin Film Battery Using LISIPON Electrolyte and Si-V Negative Electrode Films. *Electrochem. Commun.* **2003**, *5*, 32–35.
- (29) Su, Y.; Falgenhauer, J.; Leichtweiß, T.; Geiß, M.; Lupó, C.; Polity, A.; Zhou, S.; Obel, J.; Schlettwein, D.; Janek, J.; Meyer, B. K. Electrochemical Properties and Optical Transmission of High Li+Conducting LiSiPON Electrolyte Films. *Phys. Status Solidi B* **2017**, 254 (2), 1600088.
- (30) Warneke, S.; Zenn, R. K.; Lebherz, T.; Müller, K.; Hintennach, A.; Starke, U.; Dinnebier, R. E.; Buchmeiser, M. R. Hybrid Li/S Battery Based on Dimethyl Trisulfide and Sulfurized Poly-(Acrylonitrile). *Adv. Sustain. Syst.* **2018**, *2* (2), 1700144.
- (31) Zu, C. X.; Li, H. Thermodynamic Analysis on Energy Densities of Batteries. *Energy Environ. Sci.* **2011**, *4* (8), 2614–2624.
- (32) Wang, S.; Ding, Y.; Zhou, G.; Yu, G.; Manthiram, A. Durability of the Li1+xTi2-XAlx(PO4)3 Solid Electrolyte in Lithium-Sulfur Batteries. ACS Energy Lett. 2016, 1 (6), 1080–1085.
- (33) Goodenough, J. B.; Kim, Y. Challenges for Rechargeable Batteries. *J. Power Sources* **2011**, *196*, 6688.
- (34) Manthiram, A.; Fu, Y.; Chung, S. H.; Zu, C.; Su, Y. S. Rechargeable Lithium-Sulfur Batteries. *Chem. Rev.* 2014 1141175111787.
- (35) Wang, L.; Wang, Y.; Xia, Y. A High Performance Lithium-Ion Sulfur Battery Based on a Li 2S Cathode Using a Dual-Phase Electrolyte. *Energy Environ. Sci.* **2015**815511558.
- (36) Manthiram, A.; Yu, X.; Wang, S. Lithium Battery Chemistries Enabled by Solid-State Electrolytes. *Nat. Rev. Mater.* **2017**, 2 (4), 16103.
- (37) Tarascon, J. M.; Armand, M. Issues and Challenges Facing Rechargeable Lithium Batteries. In Materials for Sustainable Energy: A Collection of Peer-Reviewed Research and Review Articles from Nature Publishing Group; 2010, pp 171–179. DOI: 10.1142/9789814317665 0024.
- (38) Zhang, X.; Temeche, E.; Laine, R. M. Design, Synthesis, and Characterization of Polymer Precursors to LixPON and LixSiPON Glasses: Materials That Enable All-Solid-State Batteries (ASBs). *Macromolecules* **2020**, 53 (7), 2702–2712.
- (39) Laine, R. M.; Sellinger, A. Si-Containing Ceramic Precursors. In *The Chemistry of Organic Silicon Compounds*; 2003 DOI: 10.1002/0470857250.ch39.
- (40) Yi, J.; Liu, X.; Guo, S.; Zhu, K.; Xue, H.; Zhou, H. Novel Stable Gel Polymer Electrolyte: Toward a High Safety and Long Life Li-Air Battery. ACS Appl. Mater. Interfaces 2015, 7 (42), 23798–23804.
- (41) Levchik, S. V.; Levchik, G. F.; Balabanovich, A. I.; Weil, E. D.; Klatt, M. Phosphorus Oxynitride: A Thermally Stable Fire Retardant

- Additive for Polyamide 6 and Poly(Butylene Terephthalate). Angew. Makromol. Chem. 1999, 264 (1), 48-55.
- (42) Larson, R. W.; Day, D. E. Preparation and Characterization of Lithium Phosphorus Oxynitride Glass. *J. Non-Cryst. Solids* **1986**, 88 (1), 97–113.
- (43) Mascaraque, N.; Fierro, J. L. G.; Durán, A.; Muñoz, F. An Interpretation for the Increase of Ionic Conductivity by Nitrogen Incorporation in LiPON Oxynitride Glasses. *Solid State Ionics* **2013**, 233, 73–79.
- (44) Fleutot, B.; Pecquenard, B.; Martinez, H.; Letellier, M.; Levasseur, A. Investigation of the Local Structure of LiPON Thin Films to Better Understand the Role of Nitrogen on Their Performance. *Solid State Ionics* **2011**, *186* (1), 29–36.
- (45) Pichonat, T.; Lethien, C.; Tiercelin, N.; Godey, S.; Pichonat, E.; Roussel, P.; Colmont, M.; Rolland, P. A. Further Studies on the Lithium Phosphorus Oxynitride Solid Electrolyte. *Mater. Chem. Phys.* **2010**, *123*, 231.
- (46) Stallworth, P. E.; Vereda, F.; Greenbaum, S. G.; Haas, T. E.; Zerigian, P.; Goldner, R. B. Solid-State NMR Studies of Lithium Phosphorus Oxynitride Films Prepared by Nitrogen Ion Beam-Assisted Deposition. *J. Electrochem. Soc.* **2005**, *152* (3), A516–A522.
- (47) Wang, B.; Chakoumakos, B. C.; Sales, B. C.; Kwak, B. S.; Bates, J. B. Synthesis, Crystal Structure, and Ionic Conductivity of a Polycrystalline Lithium Phosphorus Oxynitride with the γ -Li3PO4 Structure. *J. Solid State Chem.* **1995**, *115*, 313–323.
- (48) Roh, N. S.; Lee, S. D.; Kwon, H. S. Effects of Deposition Condition on the Ionic Conductivity and Structure of Amorphous Lithium Phosphorus Oxynitrate Thin Film. *Scr. Mater.* **1999**, 42 (1), 43–49.
- (49) Meda, L.; Maxie, E. E. Lipon Thin Films Grown by Plasma-Enhanced Metalorganic Chemical Vapor Deposition in a N 2-H 2-Ar Gas Mixture. *Thin Solid Films* **2012**, *520* (6), 1799–1803.
- (50) Hu, Z.; Li, D.; Xie, K. Influence of Radio Frequency Power on Structure and Ionic Conductivity of LiPON Thin Films. *Bull. Mater. Sci.* **2008**, *31*, 681–686.
- (51) Bachman, J. C.; Muy, S.; Grimaud, A.; Chang, H. H.; Pour, N.; Lux, S. F.; Paschos, O.; Maglia, F.; Lupart, S.; Lamp, P.; Giordano, L.; Shao-Horn, Y. Inorganic Solid-State Electrolytes for Lithium Batteries: Mechanisms and Properties Governing Ion Conduction. *Chem. Rev.* **2016**, *116* (1), 140–162.
- (52) West, W. C.; Whitacre, J. F.; Lim, J. R. Chemical Stability Enhancement of Lithium Conducting Solid Electrolyte Plates Using Sputtered LiPON Thin Films. *J. Power Sources* **2004**, *126*, 134–138. (53) Hu, M.; Pang, X.; Zhou, Z. Review Recent Progress in High-Voltage Lithium Ion Batteries. *J. Power Sources* **2013**, *237*, 229.
- (54) Masquelier, C.; Croguennec, L. Polyanionic (Phosphates, Silicates, Sulfates) Frameworks as Electrode Materials for Rechargeable Li (or Na) Batteries. *Chem. Rev.* **2013**, *113* (8), 6552–6591.
- (55) Bieker, G.; Winter, M.; Bieker, P. Electrochemical in Situ Investigations of SEI and Dendrite Formation on the Lithium Metal Anode. *Phys. Chem. Chem. Phys.* **2015**, *17*, 8670–8679.
- (56) Albertus, P.; Babinec, S.; Litzelman, S.; Newman, A. Status and Challenges in Enabling the Lithium Metal Electrode for High-Energy and Low-Cost Rechargeable Batteries. *Nat. Energy* **2018**, *3* (1), 16.
- (57) Zhang, S. S.; Xu, K.; Jow, T. R. The Low Temperature Performance of Li-Ion Batteries. *J. Power Sources* **2003**, *115*, 137–140. (58) Su, Y.; Falgenhauer, J.; Polity, A.; Leichtweiß, T.; Kronenberger, A.; Obel, J.; Zhou, S.; Schlettwein, D.; Janek, J.; Meyer, B. K. LiPON Thin Films with High Nitrogen Content for Application in Lithium Batteries and Electrochromic Devices Prepared by RF Magnetron Sputtering. *Solid State Ionics* **2015**, 282,
- (59) Li, J.; Dudney, N. J.; Nanda, J.; Liang, C. Artificial Solid Electrolyte Interphase to Address the Electrochemical Degradation of Silicon Electrodes. ACS Appl. Mater. Interfaces 2014, 6 (13), 10083–10088
- (60) Chen, Y. T.; Jena, A.; Pang, W. K.; Peterson, V. K.; Sheu, H. S.; Chang, H.; Liu, R. S. Voltammetric Enhancement of Li-Ion

63-69.

- Conduction in Al-Doped Li₇-XLa₃Zr₂O₁₂ Solid Electrolyte. *J. Phys. Chem. C* **2017**, 121 (29), 15565–15573.
- (61) Shin, B. R.; Nam, Y. J.; Oh, D. Y.; Kim, D. H.; Kim, J. W.; Jung, Y. S. Comparative Study of TiS₂/Li-In All-Solid-State Lithium Batteries Using Glass-Ceramic Li₃PS₄ and Li₁₀GeP₂S₁₂ Solid Electrolytes. *Electrochim. Acta* **2014**, *146*, 395–402.
- (62) Frey, M.; Zenn, R. K.; Warneke, S.; Müller, K.; Hintennach, A.; Dinnebier, R. E.; Buchmeiser, M. R. Easily Accessible, Textile Fiber-Based Sulfurized Poly(Acrylonitrile) as Li/S Cathode Material: Correlating Electrochemical Performance with Morphology and Structure. ACS Energy Lett. 2017, 2 (3), 595–604.
- (63) Ma, G.; Wen, Z.; Jin, J.; Wu, M.; Wu, X.; Zhang, J. Enhanced Cycle Performance of Li-S Battery with a Polypyrrole Functional Interlayer. *J. Power Sources* **2014**, 267, 542–546.
- (64) Dokko, K.; Tachikawa, N.; Yamauchi, K.; Tsuchiya, M.; Yamazaki, A.; Takashima, E.; Park, J. W.; Ueno, K.; Watanabe, M.; Seki, S.; Serizawa, N. Solvate Ionic Liquid Electrolyte for Li-S Batteries. *J. Electrochem. Soc.* **2013**, *160* (8), A1304–A1310.
- (65) Ma, G.; Wen, Z.; Wang, Q.; Shen, C.; Jin, J.; Wu, X. Enhanced Cycle Performance of a Li-S Battery Based on a Protected Lithium Anode. *J. Mater. Chem. A* **2014**, 2 (45), 19355–19359.
- (66) Marmorstein, D.; Yu, T. H.; Striebel, K. A.; McLarnon, F. R.; Hou, J.; Cairns, E. J. Electrochemical Performance of Lithium/Sulfur Cells with Three Different Polymer Electrolytes. *J. Power Sources* **2000**, 89 (2), 219–226.